# Third-Generation Light-Driven Symmetric Molecular Motors

Jos C. M. Kistemaker, Peter Štacko, Diederik Roke, Alexander T. Wolters, G. Henrieke Heideman, Mu-Chieh Chang, Pieter van der Meulen, Johan Visser, Edwin Otten,[ID] and Ben L. Feringa*[ID]

Centre for Systems Chemistry, Stratingh Institute for Chemistry and Zernike Institute for Advanced Materials, Faculty of Mathematics and Natural Sciences, University of Groningen, Nijenborgh 4, 9747 AG Groningen, The Netherlands

Ⓢ Supporting Information

ABSTRACT: Symmetric molecular motors based on two overcrowded alkenes with a notable absence of a stereogenic center show potential to function as novel mechanical systems in the development of more advanced nanomachines offering controlled motion over surfaces. Elucidation of the key parameters and limitations of these third-generation motors is essential for the design of optimized molecular machines based on light-driven rotary motion. Herein we demonstrate the thermal and photochemical rotational behavior of a series of third-generation light-driven molecular motors. The steric hindrance of the core unit exerted upon the rotors proved pivotal in controlling the speed of rotation, where a smaller size results in lower barriers. The presence of a pseudo-asymmetric carbon center provides the motor with unidirectionality. Tuning of the steric effects of the substituents at the bridgehead allows for the precise control of the direction of disrotary motion, illustrated by the design of two motors which show opposite rotation with respect to a methyl substituent. A third-generation molecular motor with the potential to be the fastest based on overcrowded alkenes to date was used to visualize the equal rate of rotation of both its rotor units. The autonomous rotational behavior perfectly followed the predicted model, setting the stage for more advanced motors for functional dynamic systems.
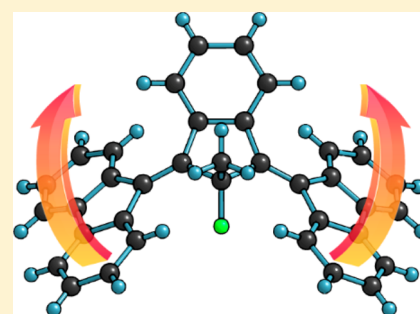
INTRODUCTION

Molecular motors and machines attract major attention, as the introduction of dynamic properties enables a wide range of responsive functions and adaptive properties in synthetic materials.[1−6] Toward the design of dynamic functional systems, the use of light as an external stimulus offers particular advantages. Photochromic systems arguably have the benefit of non-invasive triggering with the potential of high spatial-temporal precision.[7,8] Switching between two or more states upon irradiation at different wavelengths (UV/vis) can be combined with other effectuators (temperature, pH, metal-ion binding, redox) to arrive at multiresponsive behavior.[9−13] Prominent classes of photochemical switches include dithienylethenes,[14] stilbenes,[15,16] fulgides and fulgimides,[17] spiropyran,[18] DASA,[19] or azobenzenes.[20,21] Stilbenes in particular, though rather easy to prepare, suffer from the undesired thermal cis−trans isomerizing and degradation due to ring closing and oxidation toward phenanthrene (Figure 1a).[15,16] One of the major interests in our group has been the synthetic manipulation of stilbenes in order to achieve stability and increase quantum yield, control over irradiation wavelengths, and directionality of motion upon isomerization, and furthermore structural modifications to prevent decomposition.[22]

An important synthetic adjustment of a stilbene-like system (Figure 1b) was achieved by Feringa and Wynberg, introducing steric overcrowding at the alkene to form thermally stable chiral forms. This was accomplished through the presence of naphthalene moieties and aliphatic rings at both sides of the
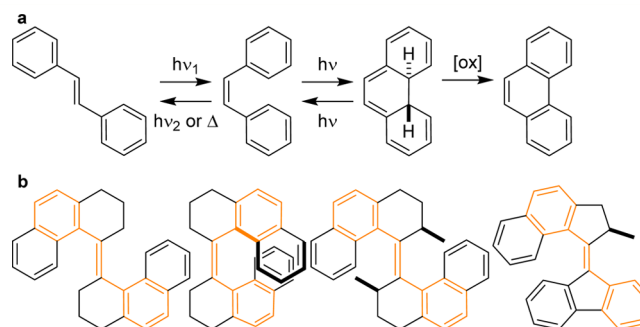

Figure 1. (a) Stilbene cis−trans isomerization and degradation due to ring closing and oxidation. (b) From left to right: stable switch, first-generation molecular motor, and second-generation molecular motor.

central alkene to prevent ring closing.[23] The introduction of stereogenic centers in these systems (Figure 1b) originally served the purpose of proving the absolute stereochemistry of its analogues.[24] However, the molecules were found to have a surprising new property: they are able to undergo a 360° unidirectional rotation around the alkene bond.[25] These systems, as a result of successive alterations, became the basis of the first-generation synthetic molecular motors, characterized by their C_2 symmetry and its principal axis at the double bond connecting upper and lower halves. Recently, functional

analogues of these first-generation synthetic motors showed potential in asymmetric catalysis[26] and control of dynamic chirality[27] and as chiral hosts.[28]

In subsequent studies, one half of these new dynamic molecules was symmetrized in order to increase their speed and quantum yield as well as allowing surface assembly.[29−31] Synthetic modifications were introduced to illustrate that these motors can perform work.[32] The desymmetrized synthetic unidirectional motors with only one stereogenic center in the upper half and a symmetric lower half were adopted as second-generation molecular motors, in which chirality was shown essential to ensure unidirectionality. The initial "stilbene motive" is continually shown in orange in all four structures in order to illustrate the predominant concept of the isomerizing alkene connecting two aromatic groups, Figure 1b. Not surprisingly, the question regarding the necessity of a stereogenic center for unidirectionality in rotary motion emerged. Recently, we reported a novel synthetic meso motor bearing two overcrowded alkenes and the notable absence of a stereogenic center, although a pseudo-asymmetric center is present.[33] In fact, each individual alkene still has to experience chirality in order to perform a unidirectional rotation. This so-called third-generation molecular motor (Figure 2) has two such alkene moieties with identical groups
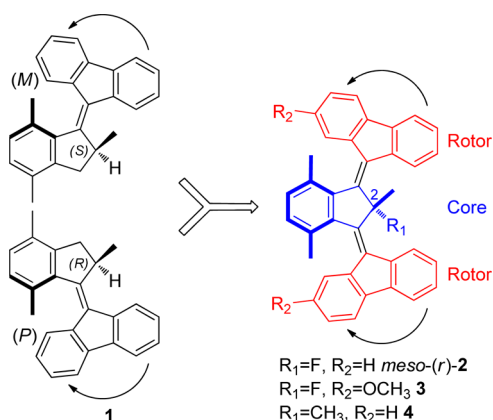
impact of the core's size on its behavior by a computational study followed by an experimental verification. Based on those results, we study the effect of the size of the substituents at the pseudo-asymmetric carbon atom (the indane bridgehead C-2, Figure 2) on the behavior of the bis-overcrowded alkenes using theoretical and experimental approaches.[34−38] After identifying the most desirable structural features, we choose a suitable candidate as a model compound for proving the persistence of unidirectionality in ultrafast third-generation molecular motors.

■ RESULTS AND DISCUSSION

Previously, unidirectional rotation has been established for motor **2** taking advantage of its desymmetrized analogue **3**.[33] For purposes of developing more advanced nanomachines and controlled motion along surfaces, the ability to tune the rotary speed is considered highly beneficial.[32,39] We therefore instigated a theoretical study on double overcrowded alkenes with a substitution pattern of two methyl groups on C-2 (R_1 = CH_3) such as **4** for maximum simplicity. Besides **4**, four more structural units were selected starting with a benzene instead of xylene moiety in the core (**5**), a *p*-difluorobenzene (**6**), a *p*-dimethoxybenzene (**7**), and one where the core xylene moiety is replaced with a phenanthrene moiety (**8**) (Chart 1).

Chart 1. Double Overcrowded Alkenes with Modified Core Moieties Featuring Benzene (5), *p*-Difluorobenzene (6), *p*-Dimethoxybenzene (7), and Phenanthrene (8)

5   6   7   8

Figure 2. Schematic design of achiral motors. Merging of two enantiomers of motor **1** (opposite helicities (*P*,*M*) and central chirality (*R*,*S*) indicated) gives rise to symmetric double overcrowded alkenes **2**−**4** (pseudo-asymmetric carbon atom C-2 indicated with "2").

that can be considered mirror images of two separate second-generation motors. This third-generation motor is specially designed to maintain unidirectionality of two parallel rotors while avoiding the stereogenic element (asymmetric carbon center) known from earlier generations of motors. Both individual alkenes experience the pseudo-asymmetry of the bridge unit (e.g., CFCH$_3$ in **2**), and, due to the opposite helicity of these alkenes with respect to the bridge unit, both fluorene moieties are rotating in the same direction with respect to the core aromatic group. This symmetry property is analogous to a car driver moving forward on a road observing his right wheel turning anti-clockwise and his left wheel turning clockwise.
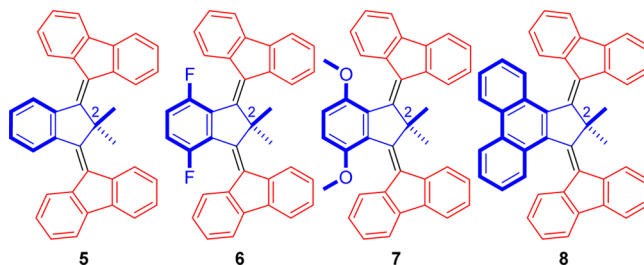
Here, we report on our investigation and characterization of the essential features of third-generation molecular motors and the limits of their performance, to finally come to demonstrate the unidirectionality of the fastest third-generation motor and potentially the fastest of all molecular rotary motors based on overcrowded alkenes designed so far. We first identify the

Theoretical Study of the Core-Size Effect. The theoretical investigation was performed using the semiempirical PM6 model to construct a potential energy surface (PES) from two dihedrals governing the aromatic planes for compounds **4**−**8** (**4** as example; Figure 3a). The resulting PES shows a two-fold symmetry with mirror planes running diagonally through the minima. The geometries of the minima and transition states (TSs) were optimized using DFT B3LYP/6-31G(d,p)[40,41] and intrinsic reaction coordinates (IRCs, **4** as example; Figure 3b) were calculated to ensure the TSs connected the identified minima. Subsequently the geometries of the minima and TSs were optimized using DFT ωB97X-D/6-31+G(d,p)[42] in dichloromethane (IEFPCM)[43,44] which revealed for each compound two global minima and two metastable local minima (minima and TSs afforded zero or one imaginary frequency, respectively, and their geometries, energies and calculated barriers are shown in Table 1). The two redundant global minima have the desired meso geometries and are close to or have C_s symmetry. The two metastable local minima were enantiomeric helical configurations and are close to or have C_2 symmetry and connected to the global minima by the calculated TSs which constitute the thermal helix inversions (THIs) known for overcrowded alkenes.

The redundant global minima possess C_s symmetry for **6** and **8** or deviate marginally from it by twisting the rotors in **4**, **5**,
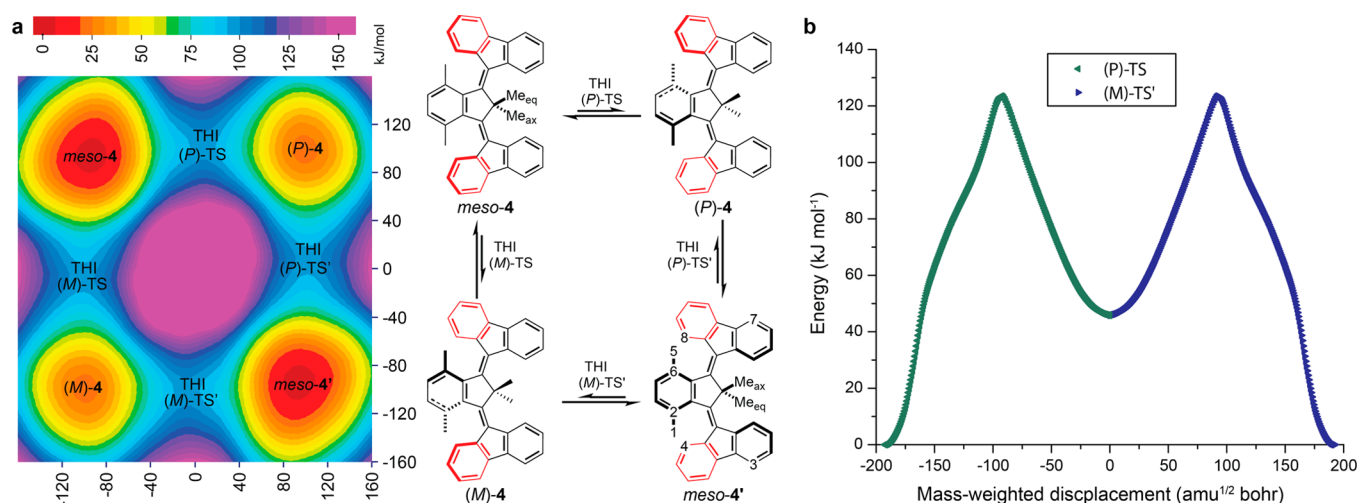
Figure 3. (a) PES of **4** (PM6, colored from 0 kJ·mol^{-1} (red) to 150 kJ·mol^{-1} (violet), x-axis: 1−2−3−4 dihedral (in °); y-axis: 5−6−7−8 dihedral (in °)), (b) IRCs of TS-**4**.

Table 1. Optimized Geometries of Minima and Transition States and Their Corresponding Gibbs Free Energies of 4−8, in kJ·mol^{-1} (DFT ωB97X-D/6-31+G(d,p) in DCM)[a]

	5	6	7	4	8
global minimum (C_s)[b]	0.0 (0.4)	0.0 (0.0)	0.0 (0.7)	0.0 (1.6)	0.0 (0.0)
helical minimum P/M (C_2)[b]	41.3 (43.9)	45.4 (50.5)	46.1 (52.2)	49.4 (56.3)	29.5 (29.5)
transition state	66.9	96.0	107	123	132
THI $C_2{\rightarrow}C_s$ T at $t_{1/2}$ = 1 h (°C)	−216	−121	−82.8	−46.6	45.5
2×THI $C_s{\rightarrow}C_s$ $T_{coalescence\ (10\ Hz)}$ (°C)[c]	44.0	182	234	310	353

[a]Geometries shown with methyl groups facing the reader, the H$_3$C−C−CH$_3$ bonds in the y−z plane, and the five-membered ring core in the x−z plane. [b]Energies in parentheses are for the symmetrical geometries. [c]Using $k = \pi\Delta\nu_0 \times 2^{-0.5}$ to provide the rate at $T_{coalescence}$. k can be used in combination with the calculated barriers to solve the Eyring equation for T.

and **7**, although not detectable by NMR due to the minute barrier of isomerization (C_s symmetric geometries are 0−1.6 kJ·mol^{-1} higher in energy, Table 1). A similar phenomenon is observed for the two metastable local minima in **4−7** which deviate slightly from C_2 symmetry by twisting one of the methyl groups on C-2 lowering the energy by 3−7 kJ·mol^{-1}. Again, this deviation from symmetry would not be observed by NMR since at room temperature the isomerization is very fast in which the averaged geometry is a C_2 symmetrical conformation. The isomerization pathway between the helical minimum and the global minimum (from now on referred to as C_2-**x** and C_s-**x**, respectively) showed increasing thermal barriers for helix inversion going from **5** < **6** < **7** < **4** < **8** which corresponds fully with the increase in size of the aromatic core moiety (Table 1). The temperature at which the half-life is 1 h (T at

$t_{1/2}$ = 1 h for THI $C_2{\rightarrow}C_s$) is a good indication of which compound would be most suitable for an NMR study. This suggests that **5−7** require very low temperatures for NMR measurements, whereas both **8** and **4** are in a temperature region where measurements can be readily performed. The two redundant meso configurations (C_s-**x** and C_s-**x**′) can interconvert through C_2-**x** by two helix inversions (2×THI, shown for **4** in Figure 3a). The barrier for this isomerization can be quantified from the approximate theoretical coalescence temperature of ^{1}H NMR resonances (CH$_3$ group resonances are calculated to be separated by ∼10 Hz, *vide infra*). From the calculated coalescence temperatures (Table 1), compound **5** appears to be the only suitable candidate for NMR investigation. To investigate the THI and 2×THI processes, compounds **4** and **5** as well as **9** were synthesized (Scheme 1).

Derivative **9** was expected to have increased solubility compared with **5** and might provide insight into substituent effects for future functionalization.

Scheme 1. Synthesis of Compounds 4, 5, and 9[a]
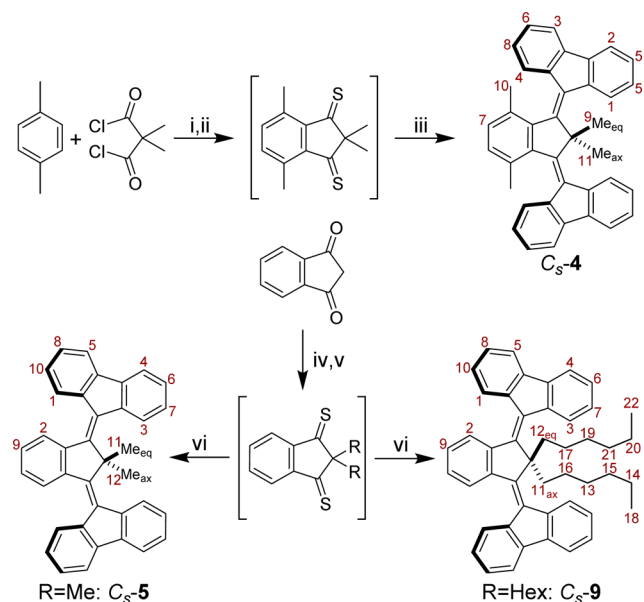
[a]Reagents and conditions: (i) AICl$_3$, CS$_2$, rt, 24 h; (ii) P$_4$S$_{10}$, toluene, reflux, 18 h; (iii) 1. 9-diazo-9*H*-fluorene, toluene, 55 °C, 48 h, 2. HMPT, 120 °C, 24 h; yields C$_s$-**4** (14% over 3 steps). R = Me: (iv) K$_2$CO$_3$, RI, CH$_3$CN, 40 °C, overnight; (v) P$_4$S$_{10}$, toluene, reflux, 18 h; (vi) 9-diazo-9*H*-fluorene, toluene, reflux, overnight; yields C$_s$-**5** (50% over 3 steps). R = Hex: (iv) K$_2$CO$_3$, RI, Aliquat 336, CH$_3$CN, 80 °C, 24 h; (iv) P$_4$S$_{10}$, Lawesson's reagent, toluene, reflux, 26 h; (iv) 9-diazo-9*H*-fluorene, toluene/tetrahydrofuran, reflux, 20 h; yields C$_s$-**9** (1% over three steps).

Experimental Study of Core Size. The synthesis of the core structure of overcrowded alkenes **4**, **5**, and **9** started with a double Friedel–Crafts acylation of dimethyl malonyl chloride on *p*-xylene afforded the bis-ketone in high yield (82%). This was transformed into the bis-thioketone by the use of phosphorous pentasulfide (97%). A Barton–Kellogg coupling of the bis-thioketone and diazofluorene followed by a desulfurization by the use of hexamethylphosphanetriamine (HMPT) yielded the desired double overcrowded alkene C$_s$-**4** (17%). For compound **5**, after double alkylation of indanedione with methyl iodide, an analogous pathway was followed where phosphorous pentasulfide was used to afford the bis-thioketone. This indanedithione underwent a Barton–Kellogg coupling with diazofluorene to give the desired product C$_s$-**5** in good overall yield (50%). Double overcrowded alkene **9** caused problems in the first step, producing significant amounts of *O*-alkylated side-product which resulted in loss of product during purification, providing the *C*-alkylated product in 9% yield. The next two steps proceeded in an analogous fashion to the synthesis of **5** affording the desired C$_s$-**9**.

The study of the photochemical and thermal isomerizations started with compound **4**, which was irradiated with UV light (365 nm in CH$_2$Cl$_2$, Figure 4a), and at room temperature no change was observed in the UV−vis absorption spectrum. Irradiation at −65 °C was accompanied by a bathochromic shift in the absorption-spectrum indicative of an increase in strain over the alkenes pointing to the formation of a metastable intermediate. After irradiation to the photostationary state (PSS), the sample was allowed to warm up to rt and full reversal to the original spectra was observed. Three cycles of irradiation at low temperature and heating at ambient temperatures did not reveal any signs of fatigue. During both of these processes an isosbestic point was observed at the same wavelength (459 nm), indicating the absence of side reactions during these first order reactions. ^{1}H NMR confirmed the identity of the stable global minimum as C$_s$-**4** by the presence of three distinct methyl resonances, which is expected of a C$_s$ symmetrical configuration of **4** but not of C$_2$ (Figure 4b, H^9,H^{10},H^{11}; assignments in Scheme 1). Irradiation to PSS at low temperatures revealed the metastable state possessing a C$_2$ symmetrical configuration, corresponding to C$_2$-**4**. Following the integrals of the NMR-resonances of H^1 over time at different temperatures enabled the construction of an Eyring plot (Figure 4c) which provided the energies of activation ($\Delta^{\ddagger}H°$ 63.2 ± 1.6 kJ·mol^{-1}, $\Delta^{\ddagger}S°$ = −17.3 ± 7.0 J·K^{-1}·mol^{-1}, $\Delta^{\ddagger}G°$ = 68.3 ± 0.5 kJ·mol^{-1}, $t_{1/2}$ = 1 h at T = −59.4 ± 0.3 °C) in reasonable agreement with the calculated barrier ($\Delta^{\ddagger}H°_{calc}$ = 70.3 kJ·mol^{-1}, $\Delta^{\ddagger}S°_{calc}$ = −10.6 J·K^{-1}·mol^{-1}, $\Delta^{\ddagger}G°_{calc}$ = 73.4 kJ·mol^{-1}).
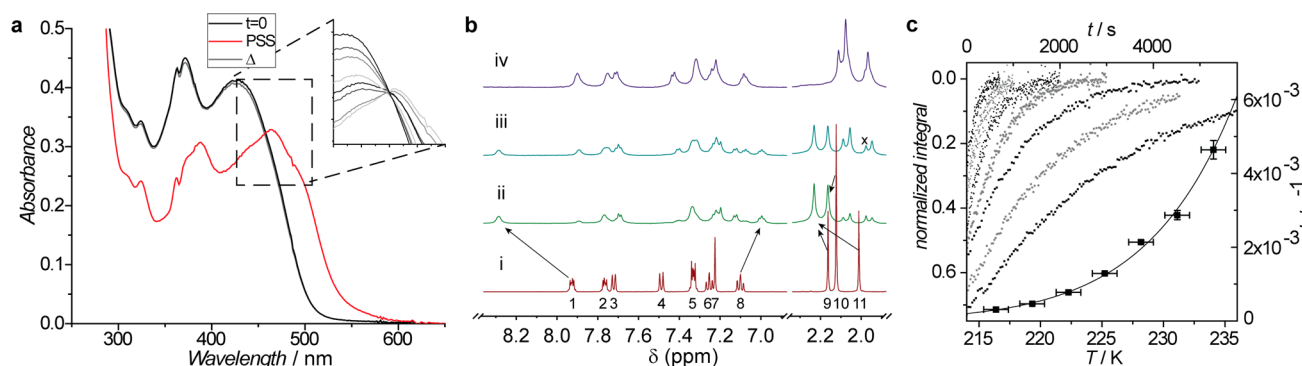

Figure 4. Thermal behavior of **4**. (a) UV−vis absorption spectrum of C$_s$-**4** in CH$_2$Cl$_2$ at rt, irradiation (365 nm, 30 min) to PSS at −65 °C and warming to rt (insert: isosbestic point at 459 nm with absorptions during both processes added). b) i: ^{1}H NMR spectrum of C$_s$-**4** (CD$_2$Cl$_2$, 500 MHz, rt), assignment in Scheme 1. ii: Transferred to a Shigemi tube and irradiated in NMR to PSS (CD$_2$Cl$_2$, 365 nm, 12 min, 600 MHz, −58 °C). iii: t = 30 min (CD$_2$Cl$_2$, 600 MHz, −58 °C). iv: t = 8 h (CD$_2$Cl$_2$, 600 MHz, −58 °C, x = impurity, presumably acetonitrile). c) Exponential decay curves of the normalized integrals of H$^1_{C_2\text{-}4}$ over time (left and top axis) and Eyring plot with error bars of 3σ (right and bottom axis).

Irradiation of double alkene C_s-**5** in *n*-pentane at −60 °C did not show any shift in the UV−vis absorption spectrum (see Supporting Information for the UV−vis spectrum) which indicates that either C_s-**5** does not undergo a double bond isomerization or more likely the thermal barrier for reversion of C_2-**5** to C_s-**5** is too low to observe the metastable species at that temperature. The barrier for THI at room temperature was calculated to be 25.6 kJ·mol^{-1} (*vide supra*) which would allow for a lifetime of 2 ns at −60 °C and a temperature of −215 °C would be required to allow for a lifetime of 1 h. Due to the low barrier for THI, C_2-**5** is not expected to be observed over the experimental temperature range. Photocyclization has been a problem for an overcrowded alkene without functional groups in the fjord region;[45] however, no photocyclization was observed in the case of compound **5** probably due to insufficient π-orbital overlap. Moreover, no other photochemistry was observed, such as described for 1,2-distyrylbenzene derivatives,[46] likely due to the rigid cyclopentane. An NMR study confirms the identity of the stable global minimum C_s-**5** by the presence of two distinct methyl resonances, which is expected of a C_s symmetrical conformation of **5** but not of C_2. This is corroborated by the calculated ^{1}H NMR spectrum of C_s-**5** (DFT giao mPW1PW91/6-311+G(2d,p) in CHCl$_3$) which strongly agrees with the experimental spectrum (Figure 5).
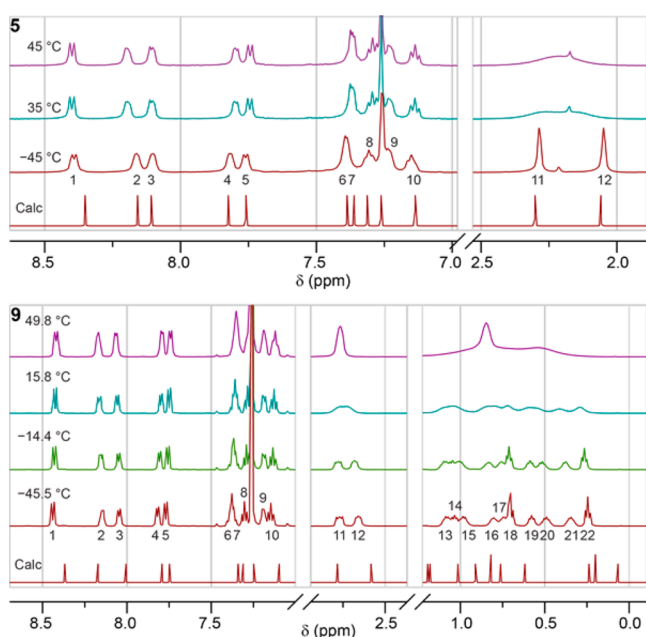

Figure 5. Temperature-dependent experimental and calculated ^{1}H NMR spectra of C_s-**5** and C_s-**9**.

Upon an increase in temperature, coalescence of the methyl resonances is observed, indicative of the two-step process in which the Me$_{eq}$ (H^{11}) and Me$_{ax}$ (H^{12}) exchange environment through a double helix inversion. The barrier determined by NMR ($\Delta^{\ddagger}G$ = 62.5 ± 1.0 kJ·mol^{-1}) is found to be lower than the computed barrier ($\Delta^{\ddagger}G°_{calc}$ = 66.9 kJ·mol^{-1}, *vide supra*), probably due to a deviation in the calculated entropy term as was observed for **4**. However, it still suggests that at these temperatures the redundant isomers C_s-**5** and C_s-**5**′ exchange through thermal processes as shown for **4** in Figure 3a.

To investigate these processes in greater detail compound **9** (Scheme 1) has been synthesized which is expected to show behavior similar to **5** but with a significantly increased solubility.

Low temperature UV−vis and NMR displayed a similar absence of change under irradiation and, similar to C_s-**5**, presence of C_s symmetry for compound **9** was shown by NMR (Figure 5; see Supporting Information for UV−vis and ^{13}C NMR spectra). An interesting pattern was observed for the ^{1}H NMR resonances of the alkyl chains of C_s-**9**. The first methylene on each alkyl displayed a similar significant downfield shift like the methyl groups of C_s-**5**, but here the strongest shift was observed for the pseudo-axial methylene group (H^{11}) instead of the pseudo-equatorial methyl in C_s-**5** (H^{11}). Due to their distinct chemical environments, the two different alkyl chains follow a peculiar pattern with methylene groups of the equatorial alkyl chain exhibiting large upfield shifts. A theoretical study of several rotamers of the alkyl chains of C_s-**9** and calculation of their average ^{1}H NMR spectrum provided a strong agreement with the experimental spectrum (R^2= 0.999, Figure 5, see Supporting Information for details). Increasing the temperature caused coalescence of the alkyl groups most apparent for the resonances of H^{11}−H^{12} at ∼2.7 ppm. This allowed for the determination of the barrier for thermal isomerization ($\Delta^{\ddagger}G$ = 59.4 ± 1.0 kJ·mol^{-1}) which again is lower than the computed barrier ($\Delta^{\ddagger}G°_{calc}$ = 65.7 kJ·mol^{-1}, $\Delta^{\ddagger}H°_{calc}$ = 51.7 kJ·mol^{-1}).

Conclusive information on the configuration of **9** came from X-ray crystallography. Crystals suitable for X-ray diffraction studies were grown by layered diffusion of a concentrated solution of **9** in dichloromethane on top of which volumes of, successively, pentane, heptane, and methanol were layered. The structure determination shows that there are two independent molecules in the unit cell (Figure 6; see Supporting
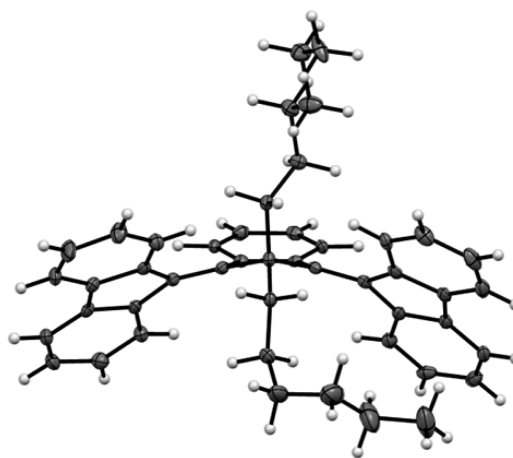

Figure 6. Molecular structure of C_s-**9** by crystallography (only one of the two independent molecules is shown).

Information for complete unit cell), which have similar metrical parameters. Both have approximate C_s symmetry (meso configuration) around the core of the bis-overcrowded alkene **9**. The alkyl group in the equatorial position is in both cases rotated such that the last three C-atoms of the hexyl chain are located directly above the plane of the fluorene ring, with C$_{hexyl}$−fluorene distances of 3.577−4.073 Å. This conformation of the equatorial alkyl group agrees with its anomalous upfield shift observed in the ^{1}H NMR spectrum. It is unclear, however, whether this *folding* in the solid state is due to packing effects or represents a genuine attractive interaction (see Supporting Information for a computational conformational study).

Conclusions on the Influence of Core Size. Molecular motors based on double overcrowded alkenes with a benzene moiety in the core show the potential to be significantly faster than those with a substituted benzene group. However, compounds **4**−**9** with C_s symmetrical stable meso states do not possess a preference for either of the two redundant geometries and therefore no preference for which of the two states undergoes a photochemical E−Z (PEZ) isomerization. The metastable helical states possess C_2 symmetry and therefore both rotors show an equal probability for undergoing a THI. Due to the redundancy of the stable states and the C_2 symmetry of the metastable state these rotors do not prefer a specific direction and are therefore not unidirectional. On account of the symmetry of the stable state it is expected that a PEZ isomerization of C_s-**9** will produce a photostationary state (PSS) between C_s-**9** and racemic C_2-**9** (Figure 7). This
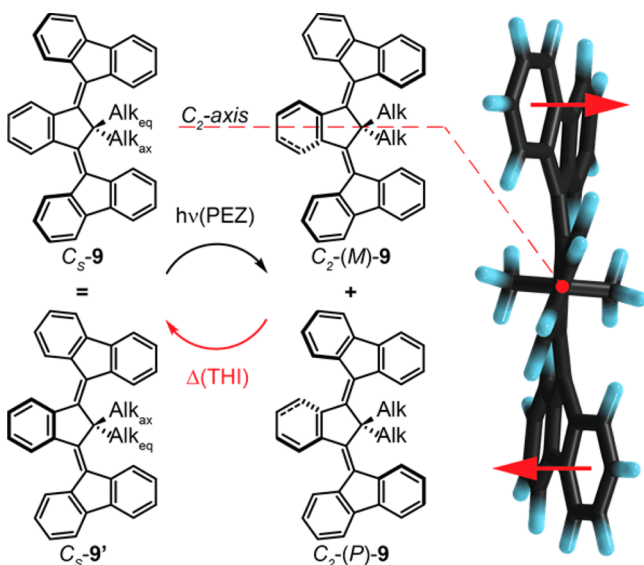

Figure 7. Rotational behavior of **9** shown (**4** and **5** behave in the same way). C_s-**9** = C_s-**9′**, produces a racemic mixture of C_2-(M)-**9** and C_2-(P)-**9** upon photochemical E−Z isomerization. For C_2-(M)-**9** the C_2 axis is indicated by the red dashed line and red dot on the calculated geometry on which the red arrows indicate the movement of the rotors for the two redundant thermal helix inversions.

isomerization yields a rotation of one of the rotors on C_s-**9** and a rotation of one of the rotors on C_s-**9′**, in opposite direction with respect to C_s-**9**. The metastable C_2-**9** undergoes a THI of either of the rotors without preference because its C_2 symmetry as indicated in Figure 7, producing equal amounts of C_s-**9** and C_s-**9′**. Over two rotational steps (PEZ−THI) the rotations sum up to a net rotation of zero due to the lack of unidirectionality. This behavior is expected for all compounds with equally sized substituents at the bridgehead position such as **4** and **5**. To achieve unidirectional rotation, a form of asymmetry has to be reintroduced like in **2** and **3**, which is achieved by substituting two differently sized moieties at the indane bridgehead (carbon 2, Chart 1) making it a pseudo-asymmetric carbon atom.[34−38]

Theoretical Study of the Substituent Effect. Several substitution patterns on the indane bridgehead were considered and investigated computationally. Certain sterically interesting substituents such as *tert*-butyl (large) and hydrogen and methoxy (smaller than methyl) were disregarded on account

of their synthetic demand and the expected chemically unstable nature of the resulting double overcrowded alkene. Note that for instance compound **2** (R₁ = H, Figure 2), featuring a hydrogen in a double allylic position can readily undergo 1,3-H-shift removing the pseudo-asymmetric center. After initial calculations on multiple double overcrowded alkenes (DFT B3LYP/6-31G(d,p),) five were selected (**18**−**22**) and studied in depth (DFT ωB97X-D/6-31+G(d,p) in DCM, Table 2). For an additional side-view perspective of the meso geometries of **18**−**22** as well as the calculated enthalpies, see the Supporting Information.

The three possible combinations of a methyl, an alkyl, and a phenyl group (compounds **18**−**20**) were selected because of their interesting potential balance in steric effects. Both the phenyl and the alkyl moieties have been reported to be slightly or significantly larger than the methyl group,[35,47,48] though there are instances in which the methyl group has been reported to exhibit a similar or larger steric effect.[49−52] The sterically demanding isopropyl group (compound **21**) and small fluorine atom (compound **22**) were selected to realize the largest difference in steric effect with respect to a methyl group. For each compound four minima were calculated, similar to **4**−**8** (*vide supra*), of which two were the enantiomeric helical metastable forms and two were found to represent the stable meso isomers with either an *r* or *s* configuration at the pseudo-asymmetric carbon atom.[34−38,53] Note that, similar to **4**−**7** (*vide supra*, Table 1), the calculated minima geometries for *r*-**18**−**22** and *s*-**18**−**22** deviate slightly from true C_s symmetry by small twists of substituents or rotors, as can be clearly observed for *s*-**18** and *r*-**21**. As before, this is not expected to be detectible by NMR due to the low barrier of isomerization which goes through the true C_s symmetrical geometry (energies shown in parentheses in Table 2).

For motors **2** and **3** it was shown that the larger substituent prefers a pseudo-axial orientation, with the rotor moieties *pinching* the substituent in the pseudo-equatorial orientation.[33] The change from a xylene core as in **4** to a benzene core in **5** increases the pinching effect of the rotors (Table 1), and the preference for the larger substituent to adopt the pseudo-axial orientation is therefore expected to remain present. To exemplify, in *r*-**18**, *r*-**19**, *r*-**21** and *r*-**22** the pseudo-axial orientation is occupied by the methyl group. The larger substituents in **21** and **22** are the isopropyl group and the methyl group, respectively, and calculations show a preference for these groups to adopt the pseudo-axial orientation with *s*-**21** and *r*-**22** being lower in energy than their corresponding diastereomer (Table 2). The calculations presented in Table 2 also show a preference for *r*-**18**, *r*-**19** and *s*-**20** over their corresponding diastereomer, which suggest the following order for steric effects in these molecules: Me > Ph > alkyl.

The barriers for THI of metastable P/M-**18**−**22** are calculated to be very low (19.1, 27.7, 21.6, 50.2, and 16.7 kJ·mol⁻¹, respectively), which makes a PEZ−THI sequence difficult to detect by conventional UV−vis or NMR techniques. The barrier for THI for **21** might be the highest for these overcrowded alkenes, although it would still require a temperature of −113 °C to obtain a half-life of 1 h. The calculated barrier of metastable P/M-**22** to *r*-**22** predicts it to be the fastest molecular motor to date with an expected half-life of only 109 ps at room temperature. The barriers for the double inversion of *s*-**18**−**22** to *r*-**18**−**22** or vice versa are calculated to be measurable by coalescence in ¹H NMR (62.9, 66.6, 66.7, 72.1, and 51.2 kJ·mol⁻¹) on the condition that both

Table 2. Structures and Optimized Geometries of Minima and Transition States and Their Corresponding Gibbs Free Energies of 18−22 (DFT ωB97X-D/6-31+G(d,p) in DCM)[a]

	18	19	20	21	22
r (C_s)	0.0 (10.6)	0.0 (0.0)	12.5 (12.5)	6.8 (55.2)	0.0 (0.1)
s (C_s)	11.6 (19.1)	9.0 (9.1)	0.0 (15.5)	0.0 (0.4)	16.2 (17.5)
helical minima P/M (C_1)	48.3	42.0	39.0	28.6	37.4
TS$_r$ $P/M{\rightarrow}r$	67.4	63.5	66.7	78.9	54.2
TS$_s$ $P/M{\rightarrow}s$	74.5	75.6	71.6	78.8	67.4

[a]Structures shown in experimentally determined most stable isomer with numbers indicating ^{1}H NMR assignments. Geometries shown with substituents facing the reader, the R−C−R bond in the $y{-}z$ plane, and the five-membered ring core in the $x{-}z$ plane. Alkyl chains of the geometries of 18 and 20 cropped to three carbons for clarity. Energies in kJ·mol^{-1}; energies in parentheses for the C_s geometries.
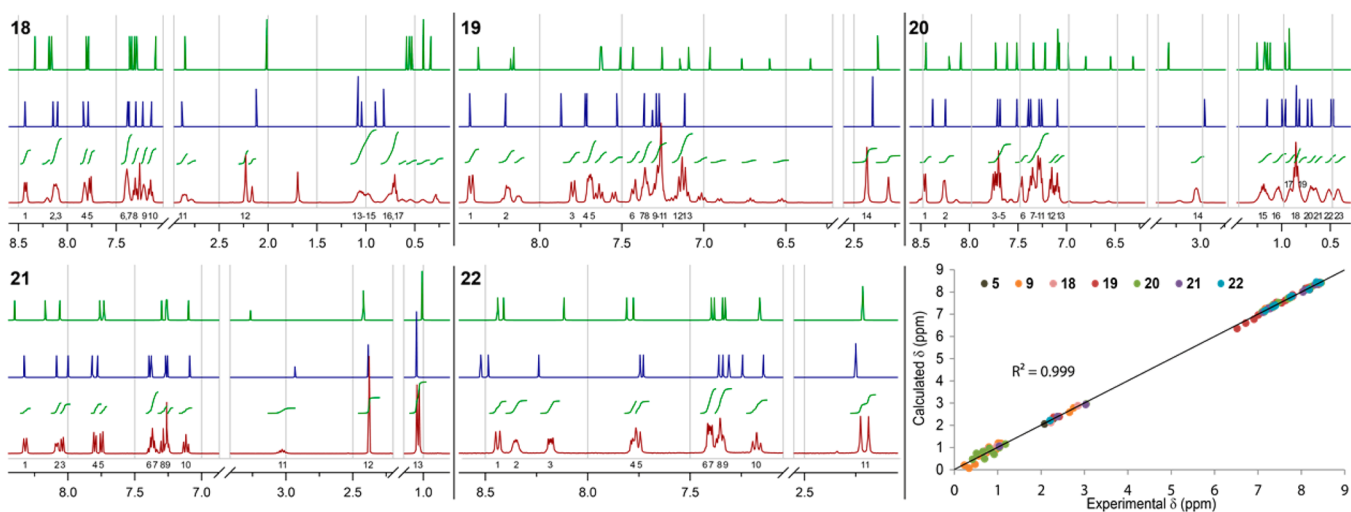

Figure 8. ^{1}H NMR spectra of **18−22**. Top: calculated spectrum of the *r*-isomer. Middle: calculated spectrum of the *s*-isomer. Bottom: experimental spectrum (CDCl$_3$) with numbering (see Table 2 for the assignments). Bottom right: correlation of experimental and calculated ^{1}H NMR chemical shifts.

diasteromers are observed. The NMR spectra of *r*-**18−22** and *s*-**18−22** were calculated (DFT giao mPW1PW91/6-311+G-

(2d,p) in CHCl$_3$, Figure 8, for enlarged spectra see the Supporting Information) in order to be able to assign the

stereoisomer of the double overcrowded alkenes which were obtained synthetically.

Experimental Study of the Substituent Effect. The double overcrowded alkenes **18−22** were all prepared following a similar route (Scheme 2). In the first step a double

Scheme 2. Synthesis of Third-Generation Molecular Motors 18−22[a]
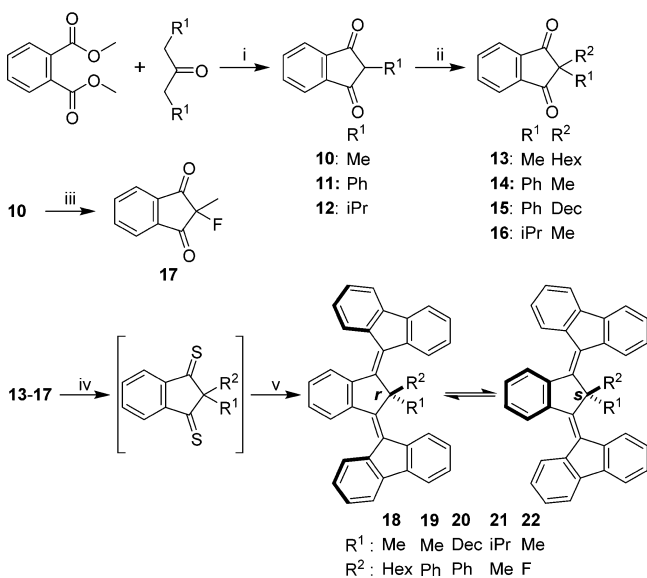
*a*Reagents and conditions: (i) NaH, toluene, 16 h, rt **10**: 63%, **11**: 31%, **12**: 87%; (ii) K$_2$CO$_3$, Aliquat 336, KF on Celite, acetonitrile, reflux, 16 h, **13**: 36%, **14**: 83%, **15**: 36%, **16**: 84%; (iii) Selectfluor, 96%; (iv) P$_4$S$_{10}$, Lawesson's reagent, toluene, 8−16 h; (v) 9-diazo-9H-fluorene, toluene, rt−reflux, 2−24 h, **18**: 66%, **19**: 23%, **20**: 24%, **21**: 3%, **22**: 14% (over iv and v).

condensation of dimethyl phthalate and symmetric ketones with the aid of sodium hydride affords the monosubstituted indanediones **10−12** in accordance with the reported literature procedures.[54−56] The second alkylation using alkyl halides on the indanediones gave rise to significant amounts of *O*-alkylated side products. This was suppressed by the use of phase transfer reagents, such as Aliquat 336, as well as the addition of potassium fluoride immobilized on Celite to the reaction mixture. The combination of both reagents afforded the highest yield and the best *C:O*-alkylated product ratio of **13−16**, which was finally further improved on using cesium carbonate instead of potassium carbonate. The fluorinated indanedione **17** was obtained from methyl-indanedione using Selectfluor. Bifunctionalized indanediones **13−17** were transformed to the corresponding indanedithiones using phosphorous pentasulfide (or a combination with Lawesson's reagent, see experimental section for details) of which most products appeared to be rather stable, probably due to a lack of hydrogens at alpha carbons. Nonetheless, the indanedithiones were directly submitted to double Barton−Kellogg couplings with diazo-fluorene to afford the desired double overcrowded alkenes **18−22** (Scheme 2).

The ^{1}H NMR spectra of **18−22** were compared to the calculated spectra and were found to be in close agreement (Figure 8). It revealed **18−20** to be present in both isomeric forms (*r*- and *s*-isomers)[38] while **21** and **22** were only found as a single isomer. At room temperature compounds **18−20** displayed coalescence of several resonances, though at low

temperature (−30 °C) the compounds entered the slow exchange region and clearly resolved ^{1}H NMR spectra were obtained. Using several 2D NMR techniques allowed for a complete proton and carbon assignment of the major isomers (see Supporting Information for all NMR spectra). The isomers of compound **18** were found in a 3.0:1.0 ratio of which the minor isomer displayed a similar effect for the hexyl chain as was observed for the pseudo-equatorially oriented hexyl chain in **9**.[53] This suggests the minor isomer to be *r*-**18** and therefore *s*-**18** to be the major isomer, which was confirmed by the comparison of the calculated ^{1}H NMR spectra to the experimental one. In this comparison, the *s* isomer strongly correlates to the major isomer of **18** and the *r* isomer correlates to the minor isomer. The presence of coalescence was predicted by calculations, however, the asymmetry in the isomer ratio makes the use of the coalescence temperature as a tool to determine the barrier for isomerization of double helix inversion slightly unreliable. Therefore, we made use of temperature dependent 1D EXSY NMR to determine the activation parameters for the exchange process (Figure 9, Table
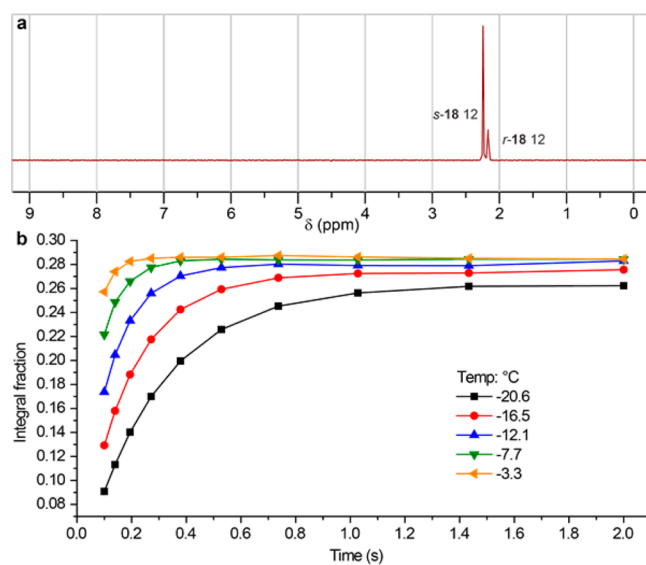

Figure 9. EXSY NMR of **18**. (a) NOESY 1D ^{1}H NMR spectrum of **18** (600 MHz, CDCl$_3$, −3.3 °C, 2 s mixing time). (b) Normalized integral of *r*-**18** at various mixing times and temperatures.

Table 3. Gibbs Free Energies of 18−20 for *r*−*s* Isomerization by EXSY NMR[a]

	18	19	20
r→*s* Δ‡G°/kJ·mol^{-1}	60.1 ± 0.3	62.3 ± 0.3	63.1 ± 1.1
s→*r* Δ‡G°/kJ·mol^{-1}	62.0 ± 0.3	63.4 ± 0.2	67.3 ± 1.1
s−*r* ΔG°/kJ·mol^{-1}	1.9 ± 0.3	1.0 ± 0.1	4.0 ± 0.2

*a*Standard state: atmospheric pressure and rt (20 °C).

3, and Supporting Information for further details), which revealed a barrier of 62.0 kJ·mol^{-1} for the isomerization of the major isomer *s*-**18** to the minor isomer *r*-**18**. The isomers of compound **19** were found in a 2.0:1.0 ratio of which the minor isomer appeared to show five distinct signals for the phenyl substituent while the major isomer showed three signals (Figure 8). This suggests that the phenyl in the major isomer is

free to rotate making the hydrogens ortho and meta to the indane bridgehead chemically identical, while in the minor isomer the orientation of the phenyl is fixed giving rise to five different resonances. In *r*-**19** the phenyl is in a pseudo-equatorial orientation, placing it in between the fluorene moieties (see the geometries in Table 2 and the Supporting Information), whereas in *s*-**19** it is oriented pseudo-axially, giving it much more spatial freedom. This suggests the assignment of the major isomer being *s*-**19** which corresponds fully with the calculated NMR spectra in which this assignment shows a far stronger correlation than the opposite combination does. EXSY NMR was again employed to determine the activation parameters for the double THI exchange process between the *s* and *r* isomers using the same method as was used for **18** (Table 3, see Supporting Information for NOESY 1D spectra and traces), revealing a similar barrier of 63.4 kJ·mol^{-1} for the isomerization of the major isomer *s*-**19** to the minor isomer *r*-**19**.

The isomers of compound **20** were found in an 8.9:1.1 ratio and for its aromatic region a nearly identical pattern is observed as was for **19**, while for the aliphatic region a similar effect is seen in the exchange of a methyl group to an alkyl as was for **5** and **9** (Figure 8). In both **5** and **19**, the pseudo-axial methyl group is shifted upfield with respect to the pseudo-equatorially oriented methyl group, while in both **9** and **20** the first methylene on the pseudo-axial alkyl group shows a downfield shift with respect to the pseudo-equatorial position.[53] With again a good correlation of the calculated spectra to the experimental ^{1}H NMR spectrum, the major isomer is assigned as *s*-**20** and the minor as *r*-**20**. EXSY NMR revealed a barrier of 67.3 kJ·mol^{-1} for the double THI exchange process going from the major isomer *s*-**20** to the minor isomer *r*-**20** (Table 3; see Supporting Information for NOESY 1D spectra and traces).

Considering the performance of overcrowded alkenes **18**−**20** as molecular motors, one should note that these systems feature reduced unidirectionality due to the presence of both isomers. Nonetheless, they still maintain preferential directionality of their rotary motion. For example, in **20** 89% rotates in one direction (counterclockwise when observed from the left in Table 2) while 11% rotates in the opposite direction resulting in a reduced unidirectional yield of 78% (determined from the *r*-**20**: *s*-**20** ratio at rt, *vide supra*). This is not an issue in **21** and **22** since they were obtained as single isomers according to ^{1}H NMR (Figure 8; note that the two resonances in the aliphatic region of **22** constitute a doublet due to F-CH$_3$ coupling, belonging to a single isomer). The size difference predicted *s*-**21** and *r*-**22** to be the most stable isomers with the larger isopropyl in the pseudo-axial orientation and the smaller fluorine in the equatorial orientation, respectively. The calculated spectra were fitted to the experimental spectra which proved the expected isomers to agree the best to the experimental spectra (Figure 8).[57]

To obtain additional information on the structure and stereochemistry of the double overcrowded alkenes, crystals suitable for X-ray diffraction analysis were grown by layered diffusion of concentrated solutions of **19**, **20**, and **22** in dichloromethane on top of which volumes of, successively, pentane, heptane, and methanol were layered (from **18** and **21** no suitable crystals were obtained). The structure determination confirmed the expected meso configuration of the bis-overcrowded alkenes, moreover, **19** and **20** were both only found with an *s* configuration at the pseudo-asymmetric carbon atom (Figure 10). While this clearly shows a preference for
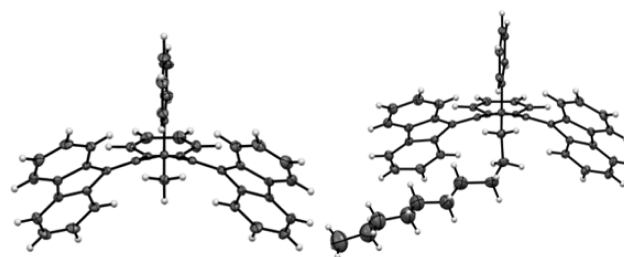

Figure 10. Molecular structures of *s*-**19** and *s*-**20** by crystallography.

both compounds to crystallize in a single configuration, it should not be used as independent proof for the assignment of the major isomer in solution since either isomer could have possessed a stronger tendency toward crystallization. However, NMR indicates only a single isomer of **22** to be present, and its X-ray analysis confirmed the computational prediction and NMR assignment, by showing **22** to possess an *r* configuration on the pseudo-asymmetric carbon atom (Figure 11).
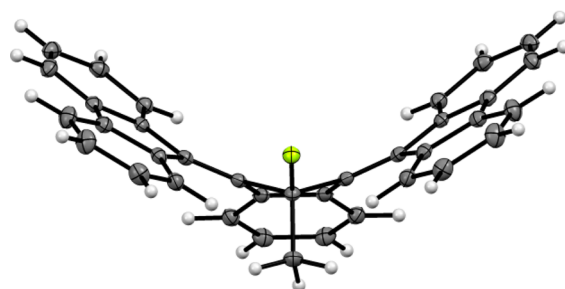

Figure 11. Molecular structure of *r*-**22** by crystallography.

Conclusions on the Influence of Substituent Size. The combined data shows the following order for steric effects of the substituents at the indane bridgehead in **18**−**22**: *i*-Pr > Ph > alkyl > Me > F. However, just based on the data for **19** and **20** (Table 3) one might expect the methyl group to be larger than the alkyl group (*s*−*r* $\Delta G°$ being smaller for **19** than for **20**) highlighting the very subtle interplay of these steric moieties with the rest of the molecule. It is also clear that this deviates from the calculated order, which predicted the steric effect of the methyl group to be larger than those of the phenyl and alkyl groups (*vide supra*). The calculated barriers for the double THI exchange process of *s*-**18**−**20** to *r*-**18**−**20** agree well with the experimental barriers ($\Delta\Delta^{\ddagger}G° = 0.9$, 3.2, and 4.3 kJ·mol^{-1}, Tables 2 and 3) while the agreement in the opposite process of *r*-**18**−**20** to *s*-**18**−**20** is much weaker ($\Delta\Delta^{\ddagger}G° = 14.4$, 13.3, and 4.0 kJ·mol^{-1}, Tables 2 and 3). To improve the correspondence between theory and experiment it might be necessary to employ different functionals, add diffuse functions or increase the basis set. The combined experimental data also confirms that in the third-generation molecular motors *s*-**21** and *r*-**22** opposite directions of rotation take place while both possess a >95% unidirectional yield (since the opposite diastereomer is not observed in ^{1}H NMR). As expected, no changes are observed in the NMR resonances at high or low temperature, or after irradiation at room or low temperature. This is due to the very low barrier for THI in combination with the symmetry of the rotors. In order to prove that these fast third-generation molecular motors are able to undergo rotation of the fluorene units under photo-irradiation, asymmetry has to be introduced in the rotor units.

Rotation of an Ultrafast Third-Generation Motor. To unequivocally demonstrate the unidirectional rotary motion, methoxy substituents were introduced in the rotor parts of the ultrafast motor with a benzene moiety as its core. Using methoxy-diazofluorene and the indanedithione of **17** in a Barton−Kellogg coupling (as in Scheme 2) afforded the desired desymmetrized double overcrowded alkene **23** as a statistical mixture of the four isomers (isomers shown in Scheme 3, for

Scheme 3. Rotational Cycle of 23
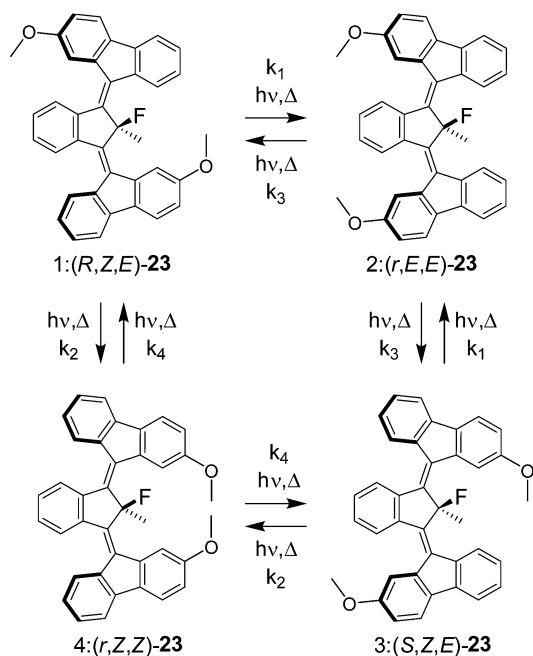
synthetic scheme see Supporting Information). This mixture was subjected to supercritical fluid chromatography (SFC) (45% 2-propanol in CO_2, Chiralpak ID at 3.5 mL·min^{-1}, 40 °C, 160 bar) which allowed the isolation of each isomer (Figure 12, isomers sequentially numbered and corresponding to the configurations numbered in Scheme 3). The four isomers are indistinguishable by UV−vis as can be seen from their nearly identical UV−vis absorption spectra (Figure 12). However, ^{19}F and ^{1}H NMR allowed for the assignment of the individual

isomers where the enantiomers of **23** (isomers 1 and 3) displayed identical NMR spectra and were assigned based on their retention time in analogy to **3**.[33] Irradiation of an isolated isomer of **23** is expected to allow it to undergo a PEZ isomerization to be directly followed by a THI. This produces the two connected isomers according to Scheme 3 in an approximate 50:50 ratio, which go on to produce both the starting isomer as well as the final isomer connected to those isomers again in a 50:50 ratio. Finally, this last isomer is formed but at the same time undergoes isomerization producing the two intermediate isomers again. The rates presented in the kinetic scheme (Scheme 3) are formulated in rate equations which were solved using matrix methods,[58] providing the following integrated rate laws (see Supporting Information for derivation and expanded formulas):

$$[(R,Z,E)\text{-}\mathbf{23}]_t = [(R,Z,E)\text{-}\mathbf{23}]_e + A_1\, e^{-k_V t} + A_2\, e^{-k_W t} + A_3\, e^{(-k_1-k_2)t} \quad (1)$$

$$[(r,E,E)\text{-}\mathbf{23}]_t = [(r,E,E)\text{-}\mathbf{23}]_e + B_1\, e^{-k_V t} + B_2\, e^{-k_W t} \quad (2)$$

$$[(S,Z,E)\text{-}\mathbf{23}]_t = [(S,Z,E)\text{-}\mathbf{23}]_e + C_1\, e^{-k_V t} + C_2\, e^{-k_W t} + C_3\, e^{(-k_1-k_2)t} \quad (3)$$

$$[(r,Z,Z)\text{-}\mathbf{23}]_t = [(r,Z,Z)\text{-}\mathbf{23}]_e + D_1\, e^{-k_V t} + D_2\, e^{-k_W t} \quad (4)$$

where $[X]_e$ describes the final concentration, k_V and k_W are compiled rate factors including k_1-k_4, A_x-D_x are compiled pre-exponential factors (including $[X]_0$ and k_1-k_4), and t is time.

Concentrated solutions in CH_2Cl_2 of the individual isomers 1−4 of **23** purged with argon were placed in the autosampler of the SFC machine, in front of which a UV lamp (365 nm) was positioned. A high concentration was used to allow the sampling to be only 4 μL, to keep the change in total volume as small as possible, and simultaneously ensuring the process lasts long enough for the collection of sufficient data. While the samples were being irradiated, aliquots for SFC analysis were taken at regular intervals, the chromatograms were integrated, and the normalized integrals were plotted against time (Figure 13).

In Figure 13 the black curves are eqs 1−4 fitted against the experimental data points by least-squares analysis in a single fit providing a small residual error and a high coefficient of
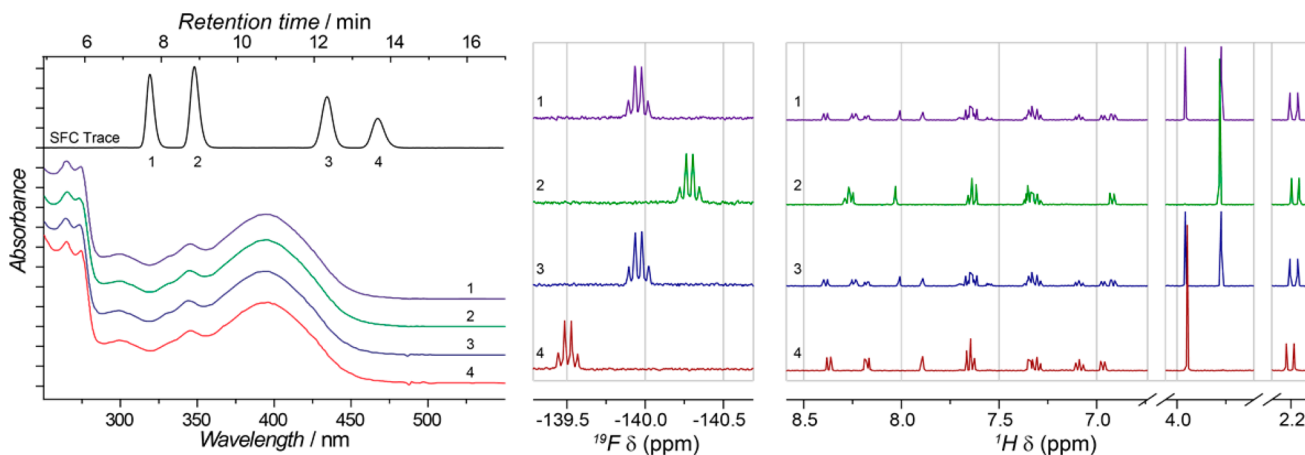

Figure 12. SFC chromatogram of **23** and the corresponding UV−vis, ^{19}F NMR, and ^{1}H NMR spectra of the individual isomers 1−4 ,with the numbering corresponding to the isomers shown in Scheme 3 (UV−vis spectra are offset for clarity).
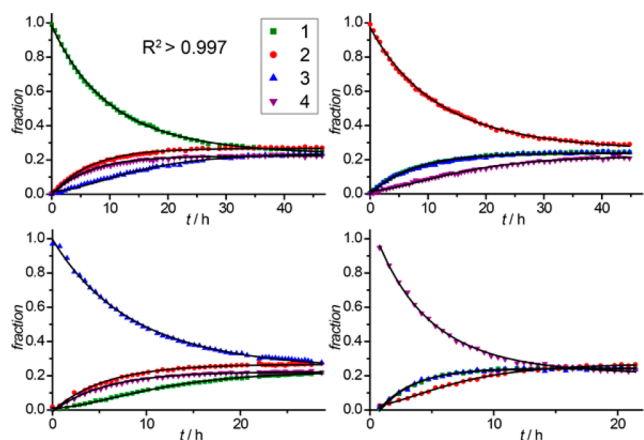
Figure 13. SFC integrals normalized over time of the four isolated isomers of **23** under 365 nm irradiation at room temperature.

determination ($R^2 = 0.997$; see Supporting Information for details of fitting). The observed behavior agrees with the proposed rate laws and proves the hypothesized connectivity as displayed in the rotational cycle in Scheme 3. Starting from any isomer of **23** there is an exponential decay of the initial isomer coupled with exponential formation of the two isomers directly connected to it, while the isomer across from the initial isomer experiences a delayed formation resulting in S-shaped curves (Figure 13).[59] Starting from the meso isomers of **23** (isomers 2 and 4) there is no preference for either of the connected isomers, expressed in nearly identical formation curves of the two enantiomeric isomers of **23** (isomers 1 and 3), while starting from one of the enantiomers, a small preference appears to exist for the formation of isomer 2 over isomer 4. This is expressed in a deviation of the final ratios from a simple statistical 1:1:1:1 ratio to a ratio of 0.99:1.11:0.99:0.90 (for isomer 1:2:3:4) starting from any of the isomers. Isomers 1 and 3 of **23** are expected to behave identically on account of their enantiomeric relationship and therefore result in identical final ratios.

All experiments result in isomer 2 $[(r,E,E)\text{-}\mathbf{23}]$ as the major isomer and isomer 4 $[(r,Z,Z)\text{-}\mathbf{23}]$ as the minor isomer (this relationship is confirmed by an ^{1}H NMR study, see Supporting Information for details). The origin of this behavior is two-fold: (i) enantiomeric isomers 1 and 3 both slightly favor rotation of one rotor over the other by 2% (normalized rates $k_1 = 1.02$ and $k_2 = 0.98$), likely due to isomers 1 and 3 being chiral and therefore possessing an asymmetric PES in the excited state, and (ii) the rate of rotation is 8% smaller for isomer 2 with respect to isomer 4 (normalized rates $k_3 = 0.91$ and $k_4 = 1.08$) leading to an accumulation of isomer 2, which could be caused by a higher quantum yield of isomer 4 with respect to isomer 2. Nonetheless, no matter what the origin of this small deviation from statistical is, it would not play a role in the third-generation motors **21** and **22** with symmetric rotors. With the use of compound **23** it is shown that, even though the thermal step is too fast to be measured in a conventional way, these motors still undergo light-driven rotation and studies using ultrafast spectroscopy to identify the metastable states and quantify the barriers involved are currently ongoing.

CONCLUSIONS

We have demonstrated the thermal and photochemical rotational behavior of a series of third-generation light-driven molecular motors. The steric hindrance around the core proved to be decisive in the tuning of the potential speed of double-overcrowded alkenes. Computational prediction of ^{1}H NMR spectra was used to support the assignment of experimental spectra as well as the relative configurations. The presence of a pseudo-asymmetric center has been shown to be essential to achieve unidirectional rotation. Careful modification of the steric bulk of the substituents on the bridgehead allows for the precise control over the direction of rotation, as clearly illustrated by the opposite directionality with respect to the methyl substituent taking place in motors **21** and **22**. Motor **22** has the potential to be the fastest unidirectional motor based on overcrowded alkenes to date, and its desymmetrization into motor **23** allowed for the visualization of the equal rate of rotation of the two rotor units, which perfectly followed the predicted model for their rotational behavior. This detailed study on elucidating key parameters for control of rotary motion of third-generation molecular motors is essential for the design of more-advanced molecular machines based on light-driven rotary motion.

ASSOCIATED CONTENT

Ⓢ Supporting Information

The Supporting Information is available free of charge on the ACS Publications website at DOI: 10.1021/jacs.7b04412.

AUTHOR INFORMATION

Corresponding Author

*b.l.feringa@rug.nl

ORCID 🄾

Edwin Otten: 0000-0002-5905-5108

Ben L. Feringa: 0000-0003-0588-8435

Notes

The authors declare no competing financial interest.

REFERENCES

(1) Astumian, R. D. *Sci. Am.* **2001**, *285*, 56−64.

(2) *Molecular Motors*; Schliwa, M., Ed.; Wiley-VCH Verlag GmbH & Co. KGaA: Weinheim, Germany, 2003.

(3) Browne, W. R.; Feringa, B. L. *Nat. Nanotechnol.* **2006**, *1*, 25−35.

(4) Balzani, V.; Credi, A.; Venturi, M. *Molecular Devices and Machines - Concepts and Perspectives for the Nanoworld*, 2nd ed.; VCH-Wiley: Weinheim, Germany, 2008.

(5) Stoddart, J. F. *Chem. Soc. Rev.* **2009**, *38*, 1802−1820.

(6) Kay, E. R.; Leigh, D. A. *Angew. Chem., Int. Ed.* **2015**, *54*, 10080−10088.

(7) Feringa, B. L.; Browne, W. R. *Molecular Switches*; Wiley-VCH Verlag GmbH & Co. KGaA: Weinheim, Germany, 2011; Vols. I and II.

(8) Göstl, R.; Senf, A.; Hecht, S. *Chem. Soc. Rev.* **2014**, *43*, 1982−1996.

(9) Fihey, A.; Perrier, A.; Browne, W. R.; Jacquemin, D. *Chem. Soc. Rev.* **2015**, *44*, 3719−3759.

(10) Qi, Q.; Qian, J.; Ma, S.; Xu, B.; Zhang, S. X.-A.; Tian, W. *Chem. - Eur. J.* **2015**, *21*, 1149−1155.

(11) Jin, P.; Cao, F.; Luo, Q. *Tetrahedron* **2016**, *72*, 5488−5494.

(12) Gallardo, I.; Guirado, G.; Hernando, J.; Morais, S.; Prats, G. *Chem. Sci.* **2016**, *7*, 1819−1825.

(13) Zheng, H.-R.; Niu, L.-Y.; Chen, Y.-Z.; Wu, L.-Z.; Tung, C.-H.; Yang, Q.-Z. *RSC Adv.* **2016**, *6*, 41002−41006.

(14) Irie, M.; Fukaminato, T.; Matsuda, K.; Kobatake, S. *Chem. Rev.* **2014**, *114*, 12174−12277.

(15) Waldeck, D. H. *Chem. Rev.* **1991**, *91*, 415−436.

(16) Meier, H. *Angew. Chem., Int. Ed. Engl.* **1992**, *31*, 1399−1420.

(17) Yokoyama, Y. *Chem. Rev.* **2000**, *100*, 1717−1740.

(18) Klajn, R. *Chem. Soc. Rev.* **2014**, *43*, 148−184.

(19) Helmy, S.; Oh, S.; Leibfarth, F. A.; Hawker, C. J.; Read de Alaniz, J. *J. Org. Chem.* **2014**, *79*, 11316−11329.

(20) *Smart Light-Responsive Materials*; Zhao, Y., Ikeda, T., Eds.; John Wiley & Sons, Inc.: Hoboken, NJ, 2009.

(21) Beharry, A. A.; Woolley, G. A. *Chem. Soc. Rev.* **2011**, *40*, 4422−4437.

(22) Cnossen, A.; Browne, W. R.; Feringa, B. L. In *Molecular Machines and Motors: Recent Advances and Perspectives*; Credi, A., Silvi, S., Venturi, M., Eds.; Springer International Publishing: Cham, 2014; pp 139−162.

(23) Feringa, B.; Wynberg, H. *J. Am. Chem. Soc.* **1977**, *99*, 602−603.

(24) Harada, N.; Koumura, N.; Feringa, B. L. *J. Am. Chem. Soc.* **1997**, *119*, 7256−7264.

(25) Zijlstra, R. W. J.; Jager, W. F.; de Lange, B.; van Duijnen, P. T.; Feringa, B. L.; Goto, H.; Saito, A.; Koumura, N.; Harada, N. *J. Org. Chem.* **1999**, *64*, 1667−1674.

(26) Wang, J.; Feringa, B. L. *Science* **2011**, *331*, 1429−1432.

(27) Zhao, D.; van Leeuwen, T.; Cheng, J.; Feringa, B. L. *Nat. Chem.* **2016**, *9*, 250−256.

(28) Wezenberg, S. J.; Vlatković, M.; Kistemaker, J. C. M.; Feringa, B. L. *J. Am. Chem. Soc.* **2014**, *136*, 16784.

(29) Koumura, N.; Geertsema, E. M.; Meetsma, A.; Feringa, B. L. *J. Am. Chem. Soc.* **2000**, *122*, 12005−12006.

(30) van Delden, R. A.; ter Wiel, M. K. J.; Pollard, M. M.; Vicario, J.; Koumura, N.; Feringa, B. L. *Nature* **2005**, *437*, 1337−1340.

(31) Pollard, M. M.; Meetsma, A.; Feringa, B. L. *Org. Biomol. Chem.* **2008**, *6*, 507−512.

(32) Kudernac, T.; Ruangsupapichat, N.; Parschau, M.; Maciá, B.; Katsonis, N.; Harutyunyan, S. R.; Ernst, K.-H.; Feringa, B. L. *Nature* **2011**, *479*, 208−211.

(33) Kistemaker, J. C. M.; Štacko, P.; Visser, J.; Feringa, B. L. B. L. *Nat. Chem.* **2015**, *7*, 890−896.

(34) Moss, G. P. *Pure Appl. Chem.* **1996**, *68*, 2214.

(35) Eliel, E. L.; Wilen, S. H. *Stereochemistry of Organic Compounds*; John Wiley & Sons: New York, 1994.

(36) Cahn, R. S.; Ingold, C.; Prelog, V. *Angew. Chem., Int. Ed. Engl.* **1966**, *5*, 385−415.

(37) Prelog, V.; Helmchen, G. *Angew. Chem., Int. Ed. Engl.* **1982**, *21*, 567−583.

(38) Per the IUPAC definition:"Pseudo-asymmetric carbon atom is the traditional name for a tetrahedrally coordinated carbon atom bonded to four different entities, two and only two of which have the same constitution but opposite chirality sense. The *r*/*s* descriptors of pseudo-asymmetric carbon atoms are invariant on reflection in a mirror (i.e. *r* remains *r*, and *s* remains *s*), but are reversed by the exchange of any two entities (i.e. *r* becomes *s*, and *s* becomes *r*)."

(39) Saywell, A.; Bakker, A.; Mielke, J.; Kumagai, T.; Wolf, M.; García-López, V.; Chiang, P.-T.; Tour, J. M.; Grill, L. *ACS Nano* **2016**, *10*, 10945−10952.

(40) Becke, A. D. *Phys. Rev. A: At., Mol., Opt. Phys.* **1988**, *38*, 3098−3100.

(41) Lee, C.; Yang, W.; Parr, R. G. *Phys. Rev. B: Condens. Matter Mater. Phys.* **1988**, *37*, 785−789.

(42) Chai, J.-D.; Head-Gordon, M. *Phys. Chem. Chem. Phys.* **2008**, *10*, 6615−6620.

(43) Miertuš, S.; Scrocco, E.; Tomasi, J. *Chem. Phys.* **1981**, *55*, 117−129.

(44) Cancès, E.; Mennucci, B.; Tomasi, J. *J. Chem. Phys.* **1997**, *107*, 3032.

(45) Geertsema, E. M.; Koumura, N.; ter Wiel, M. K. J.; Meetsma, A.; Feringa, B. L. *Chem. Commun.* **2002**, *24*, 2962−2963.

(46) Op den Brouw, P. M.; Laarhoven, W. H. *J. Org. Chem.* **1982**, *47*, 1546−1555.

(47) Hirsch, J. A. In *Topics in Stereochemistry*; Allinger, N. L., Eliel, E. L., Eds.; Interscience: New York, 1967; p 199.

(48) Taft, R. W. *J. Am. Chem. Soc.* **1952**, *74*, 2729−2732.

(49) Bott, G.; Field, L. D.; Sternhell, S. *J. Am. Chem. Soc.* **1980**, *102*, 5618−5626.

(50) Wiberg, K. B.; Hammer, J. D.; Castejon, H.; Bailey, W. F.; DeLeon, E. L.; Jarret, R. M. *J. Org. Chem.* **1999**, *64*, 2085−2095.

(51) Vicario, J.; Walko, M.; Meetsma, A.; Feringa, B. L. *J. Am. Chem. Soc.* **2006**, *128*, 5127−5135.

(52) Lunazzi, L.; Mancinelli, M.; Mazzanti, A.; Lepri, S.; Ruzziconi, R.; Schlosser, M. *Org. Biomol. Chem.* **2012**, *10*, 1847−1855.

(53) Similar to the observations for compound **9**, the alkyl chains in the pseudoequatorial orientation in *r*-**18** and *s*-**20** prefer conformations in which the chain is folded back onto the rotors over an anti conformation along the entire chain, as indicated by calculations and ^{1}H NMR spectroscopy, which shows the hydrogens of the fourth methylene group to exhibit the strongest upfield shift.

(54) Mosher, W. A.; Soeder, R. W. *J. Org. Chem.* **1971**, *36*, 1561−1563.

(55) Murthy, A. R.; Wyrick, S. D.; Hall, I. H. *J. Med. Chem.* **1985**, *28*, 1591−1596.

(56) Kuck, D.; Lindenthal, T.; Schuster, A. *Chem. Ber.* **1992**, *125*, 1449−1460.

(57) Sum of squared residuals is 6 times smaller for *s*-**21** than for *r*-**21** and 4 times smaller for *r*-**22** than for *s*-**22**.

(58) Berberan-Santos, M. N.; Martinho, J. M. G. *J. Chem. Educ.* **1990**, *67*, 375.

(59) From the rates one can determine the average amount of rotor turns in a specific period of isomerization. During the period in which it takes the isomer with delayed formation to reach 95% ($t_{95\%}$) of its final concentration, which occurs at 39, 40, 29, and 19 h for the described samples of isomers 1−4 of **23**, respectively, each motor molecule on average undergoes 2.9 isomerizations of its rotor units. This rate is fully dependent on the concentrations (which were roughly equal) and the intensity of the light source, which varied due to the setup (isomer 4: (*r,Z,Z*)-**23** was closest to the lamp in the autosampler, reflected by the lowest $t_{95\%}$). Samples of low concentration that were close to the lamp reached equilibrium conditions in the duration of a single SFC analysis (~10 min). Normalized rates are presented for clarity; see Supporting Information for rates of individual experiments.